Three-Dimensional Direct Numerical Simulation of Surface-Tension-Gradient Effects on the Leveling of an Evaporating Multicomponent Fluid

ARTICLE *in* LANGMUIR · FEBRUARY 1999

Impact Factor: 4.46 · DOI: 10.1021/la980414u

3 AUTHORS, INCLUDING:

Murat Hakki Eres
University of Southampton
41 PUBLICATIONS **415** CITATIONS
SEE PROFILE

David Weidner
University of Delaware
14 PUBLICATIONS **314** CITATIONS
SEE PROFILE

Three-Dimensional Direct Numerical Simulation of Surface-Tension-Gradient Effects on the Leveling of an Evaporating Multicomponent Fluid

M. H. Eres,* D. E. Weidner, and L. W. Schwartz

Department of Mechanical Engineering, University of Delaware, Newark, Delaware 19716

Received April 10, 1998. In Final Form: September 10, 1998

Mathematical and numerical modeling of drying coating layers is of interest to both industrial and academic communities. Compositional changes that occur during the drying process make the implementation of practical and efficient numerical models rather difficult. In this paper we present a three-dimensional mathematical and numerical model based on the lubrication approximation for the flow of drying paint films on horizontal substrates. The paint is modeled as a multicomponent liquid with one nonvolatile and one volatile component, termed the "resin" and the "solvent" respectively. Our model includes the effects of surface tension and gravitational forces as well as surface tension gradient effects which arise due to solvent evaporation. The dependence of viscosity, diffusivity, and evaporation rate on resin concentration is also incorporated in the model. A closed-form linearized solution has been found for coating layers that are of almost uniform thickness. The numerical solution agrees closely with the linear solution in the appropriate limit. A model simulation demonstrates the effect of surface tension gradients due to compositional changes in a three-dimensional flow field, and we suggest methods by which these gradients may be used to obtain a more uniform final coating layer.

1. Introduction

Many industrial processes and natural phenomena involve the flow of thin liquid films, with perhaps the most widespread industrial application being the coating of solid surfaces with a paint film. When a coating of paint is applied to a flat substrate, the initial coating will generally be uneven. It is usually desired to have a final coating that is as uniform as possible. If the function of the coating is decorative, a uniform coating will be the most aesthetically pleasing. If the purpose of the coating is protection, an uneven coating may not supply adequate protection in thin regions. Fortunately, surface tension, and sometimes gravitational forces, tends to reduce irregularities in the initial coating layer. Surface tension energies are at a minimum for a uniformly level coating layer, and if the liquid lies above a horizontal substrate, gravitational forces will move the liquid from thick regions to thin regions. Opposing these two forces is viscosity. As the solvent evaporates from the coating liquid, viscosity increases until eventually the coating layer is solid.

A simplified leveling model for the evolution of a two-dimensional, initially sinusoidal shaped coating layer was first considered by Orchard.[1] Using a linear theory, he predicted the rate of leveling as a function of the average film thickness, surface tension, viscosity, and ripple wavelength. This work was extended by Overdiep,[2] who considered the leveling behavior of solvent-based alkyd paints. He found that, for these paints, Orchard's model failed to give even a qualitative description of the leveling process. His experimental results indicated that, in the course of the leveling process, an initially sinusoidal profile would become completely horizontal. Subsequently, regions which were initially crests would become troughs, and regions which were initially troughs would form crests. This anomalous behavior could not be explained using Orchard's leveling theory. Overdiep attributed the inconsistency to the neglect of surface-tension-gradient effects in Orchard's analysis.

The surface tension of alkyd paints is a function of resin concentration, with the resin component having a higher surface tension than the solvent component. If the resin concentration varies along the layer, the surface tension will also vary. For a sinusoidal initial profile, the troughs will ultimately have a higher average resin concentration than the crests. The surface tension gradients arising from the resin concentration gradients will tend to move liquid from the crests to the troughs, thus enhancing the leveling effects of surface tension and gravity. However, unlike surface tension and gravity, surface tension gradients will continue after the layer has reached a uniform level. The liquid will continue to move toward the region that was initially a trough. Thus Overdiep explained the "rebound" effect observed experimentally. Later, this effect was also observed by Kojima *et al.*[3,4] for waterborne thermosetting coatings.

Schwartz *et al.*[5] extended Overdiep's leveling model to include the effects of surfactants. Neglecting inertial terms and employing the lubrication approximation, they derived a mathematical model for the evolution of thin liquid films and for the surface concentration of the surfactants. They apply a linearized theory to the coupled problem in order to obtain a physical insight and explain the effect of surfactants on the leveling history of the thin liquid film. Schwartz *et al.*[6] considered the effects of surfactant gradients in more detail. In that work, it was shown that the presence of surfactant slows the leveling process and that critical surfactant concentrations exist for which leveling is maximally retarded. Additionally, finite dif-

(1) Orchard, S. E. *Appl. Sci. Res. A* **1962**, *11*, 451.
(2) Overdiep, W. S. *Prog. Org. Coat.* **1986**, *14*, 159.
(3) Kojima, S.; Moriga, T.; Takenouchi, K. *Polym. Eng. Sci.* **1993**, *33* (20), 1320.
(4) Kojima, S.; Moriga, T.; S. Takenouchi, K. *Polym. Eng. Sci.* **1995**, *35* (24), 1949.
(5) Schwartz, L. W.; Weidner, D. E.; Eley, R. R. *Langmuir* **1995**, *11* (10), 3690.
(6) Schwartz, L. W.; Cairncross, R. A.; Weidner, D. E. *Phys. Fluids* **1996**, *8* (7), 1693.

10.1021/la980414u CCC: $18.00
Published on Web 02/11/1999

ference results were shown to agree with finite element method results. Howison *et al.*[7] developed a two-dimensional mathematical model for drying paint layers in terms of coating height and solvent concentration. They showed the importance of surface tension gradients in the flow history of evaporating liquid films.

The beneficial effect of surface tension, leading to more uniform coating layers, is limited largely to solid surfaces or substrates whose curvature variation is small. Indeed, in regions where the substrate is highly curved, surface tension can result in defects in the final coating: the coating tends to be thin at outside corners and to be thick or "puddled" at inside corners. The possibility that surface tension gradients could improve the uniformity of drying paint films on curved substrates was considered by Weidner *et al.*[8] In this work the canonical problem of the coating evolution of a drying, multicomponent liquid in the vicinity of a sharp corner was considered. For this type of geometry, surface tension forces will initially displace liquid from corner regions, but the thinning will produce surface tension gradients which act to pull liquid back to the corner region. If the evaporation time scale is suitably matched to the time scale for flow induced by surface tension gradients, corner defects in the final dry coating layer can be substantially mitigated.

In all the aforementioned works, only idealized two-dimensional film problems were considered. Coating problems of industrial interest are frequently three dimensional. Weidner *et al.*[9] solved numerically the coating layer evolution problem on horizontal cylinders by using an alternating-direction implicit method. Their model captures three-dimensional effects on the time history of the coating layer. However, drying and surface-tension-gradient effects are excluded from their model. In this work we seek to extend the modeling to include the effect of surface tension gradients due to compositional changes on the leveling history of initially nonuniform coating layers on horizontal substrates.

In section 2 we derive the mathematical models for the evolution of coating and resin heights, and the resin concentration. Since the viscosity, the surface tension, and the evaporation rate are all dependent on resin concentration, we also give mathematical models which describe this dependency explicitly. In section 3 these equations are nondimensionalized. We derive a linearized solution for the nondimensional problem in section 4. The numerical implementation is discussed in section 5. In section 6, we compare linearized and numerical solutions, and present results from numerical simulations using various coating parameters. Conclusions are drawn in section 7.

2. Mathematical Model

Figure 1 shows a thin liquid film coating on an impermeable horizontal substrate. Here $\tilde{x}$ is the coordinate parallel to the substrate and $\tilde{z}$ is the coordinate perpendicular to the substrate. The $\tilde{y}$ coordinate is also parallel to the substrate and points into the page. The coating height is a function of $\tilde{x}$, $\tilde{y}$, and time $\tilde{t}$; thus, $\tilde{h} = \tilde{h}(\tilde{x},\tilde{y},\tilde{t})$. The wavelength of the initial disturbance in the $\tilde{x}$ direction is $\tilde{\lambda}_{\tilde{x}}$, and the average initial coating height is $\tilde{h}^{(0)}$.

The coating is modeled as a two-component liquid composed of "resin" and "solvent." Only the solvent

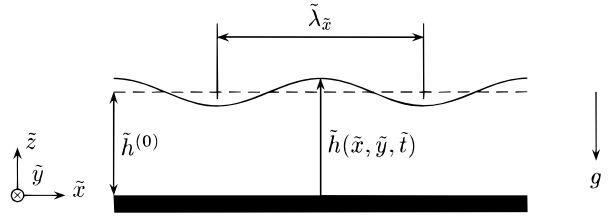

Figure 1. Schematic diagram of a thin liquid film coating on an impermeable horizontal substrate. Here, $\tilde{h}(\tilde{x},\tilde{y},\tilde{t})$ is the coating height, $\tilde{h}^{(0)}$ is the average initial coating height, g is the acceleration of gravity, and $\tilde{\lambda}_{\tilde{x}}$ is the wavelength of the initial disturbance in the $\tilde{x}$ direction.

evaporates, and as it does, the resin concentration of the bulk liquid increases. Because of the thinness of the layer, we assume that any variations in the resin concentration in the $\tilde{z}$ direction are small and consider only the layer-averaged resin fraction, which is a function of $\tilde{x}$, $\tilde{y}$, and $\tilde{t}$; thus, $c = c(\tilde{x}, \tilde{y}, \tilde{t})$. Weidner *et al.*[8] give the details of this "well-mixed" assumption. The depth-averaged viscosity $\tilde{\mu} = \tilde{\mu}(c(\tilde{x}, \tilde{y}, \tilde{t}))$, the surface tension $\tilde{\sigma} = \tilde{\sigma}(c(\tilde{x}, \tilde{y}, \tilde{t}))$, the evaporation rate, $\tilde{E} = \tilde{E}(c(\tilde{x}, \tilde{y}, \tilde{t}))$, and the diffusivity $\tilde{D} = \tilde{D}(c(\tilde{x}, \tilde{y}, \tilde{t}))$ are all dependent on the resin concentration. The density of the resin and the density of the solvent are assumed to be equal to the constant paint density.[7] We also define an imaginary thickness of the resin layer $\tilde{h}_r$ given by $\tilde{h}_r(\tilde{x},\tilde{y},\tilde{t}) = \tilde{h}(\tilde{x},\tilde{y},\tilde{t})\, c(\tilde{x},\tilde{y},\tilde{t})$, which would be the coating thickness at a given station if all the solvent in the mixture evaporated. The use of $\tilde{h}_r$ in the following derivation allows us to determine the flow history by solving two coupled partial differential equations for $\tilde{h}$ and $\tilde{h}_r$. Additionally, it enables us to write the equations in divergence form, which allows exact conservation of resin.

By exploiting the long−thin geometry of the liquid film and integrating the velocity components parallel to the substrate across the thin dimension, it is possible to extract a simpler set of equations from the rather complex vector Navier−Stokes equations. This procedure, known as the lubrication approximation,[10] leads to the following equation for the total flux

$$\tilde{Q} = \frac{\tilde{h}^2}{2\tilde{\mu}}\tilde{\nabla}\tilde{\sigma} - \frac{\tilde{h}^3}{3\tilde{\mu}}\tilde{\nabla}\tilde{p} \tag{1}$$

where $\tilde{\mathbf{Q}} = \tilde{\mathbf{Q}}(\tilde{x},\tilde{y},\tilde{t})$ is the areal flux vector with components in the $\tilde{x}$ and $\tilde{y}$ directions, $\tilde{p} = \tilde{p}(\tilde{x},\tilde{y},\tilde{t})$ is the pressure inside the coating layer relative to that of the air above, and $\tilde{\nabla} = \partial/\partial\tilde{x}\, e_{\tilde{x}} + \partial/\partial\tilde{y}\, e_{\tilde{y}}$ is the gradient operator in the direction of the unit vectors ($e_{\tilde{x}}$, $e_{\tilde{y}}$). In eq 1 we have used the shear stress condition on an arbitrary free surface

$$\tilde{\Pi}\cdot\mathbf{n}\cdot\mathbf{s} = \tilde{\nabla}_s\tilde{\sigma} \tag{2}$$

where $\tilde{\Pi}$, $\mathbf{n}$, and $\mathbf{s}$ are the stress tensor and the unit normal and tangent vectors, respectively, and $\tilde{\nabla}_s$ is the surface gradient operator.[6] For an almost flat surface, $|\tilde{\nabla}\tilde{h}| \ll 1$, the unit normal vector is $\mathbf{n} \approx e_{\tilde{z}}$, and eq 2 can be simplified to

$$\tilde{\tau}_{\tilde{z}\tilde{x}}\, e_{\tilde{x}} + \tilde{\tau}_{\tilde{z}\tilde{y}}\, e_{\tilde{y}} = \tilde{\nabla}\tilde{\sigma} \tag{3}$$

where the subscripted $\tilde{\tau}$ are components of the stress tensor. The normal stress condition on an arbitrary surface is given by

$$\tilde{\Pi}\cdot\mathbf{n}\cdot\mathbf{n} = \tilde{\sigma}\tilde{\kappa} \tag{4}$$

(7) Howison, S. D.; Moriarty, J. A.; Ockendon, J. R.; Terrill, E. L.; Wilson, S. K. *J. Eng. Math.* **1997**, *32*, 377.
(8) Weidner, D. E.; Schwartz, L. W.; Eley, R. R. *J. Colloid Interface Sci.* **1996**, *179*, 66.
(9) Weidner, D. E.; Schwartz, L. W.; Eres, M. H. *J. Colloid Interface Sci.* **1997**, *187* (1), 243.
(10) Sherman, F. S. *Viscous flow*; McGraw-Hill, Inc.: New York, 1990.

where $\tilde{\kappa}$ is the curvature of the surface. When $|\tilde{\nabla}\tilde{h}| \ll 1$, $\tilde{\kappa} \approx \tilde{\nabla}^2\tilde{h}$ and eq 4 simplifies to

$$\Delta p = \tilde{\tau}_{\tilde{z}\tilde{z}} = -\tilde{\sigma}\tilde{\nabla}^2\tilde{h}$$

where $\tilde{\nabla}^2 = \partial^2/\partial\tilde{x}^2 + \partial^2/\partial\tilde{y}^2$ is the Laplacian operator and Δp is the pressure jump across the free surface. Assuming the air above the free surface is at $p = 0$ and including gravitational forces, the pressure at the substrate in eq 1 is given by

$$\tilde{p} = -\tilde{\sigma}\tilde{\nabla}^2\tilde{h} + \rho g\tilde{h} \tag{5}$$

where ρ is the density and g is the acceleration of gravity.

Integral mass conservation requires that

$$\frac{\partial\tilde{h}}{\partial\tilde{t}} = -\tilde{\nabla}\cdot\tilde{\mathbf{Q}} - \tilde{E} \tag{6}$$

where $\tilde{\nabla}$ denotes the divergence operator and $\tilde{E}$ is the evaporation rate with units of velocity. Combining eqs 1, 5, and 6 and noting that the density ρ is constant, we obtain the governing differential equation for the time evolution of the coating height as

$$\frac{\partial\tilde{h}}{\partial\tilde{t}} = -\tilde{\nabla}\cdot\left[\frac{\tilde{h}^2}{2\tilde{\mu}}\tilde{\nabla}\tilde{\sigma} + \frac{\tilde{h}^3}{3\tilde{\mu}}\tilde{\nabla}^2\tilde{h}\tilde{\nabla}\tilde{\sigma} + \frac{\tilde{h}^3}{3\tilde{\mu}}\tilde{\sigma}\tilde{\nabla}\tilde{\nabla}^2\tilde{h} - \frac{\tilde{h}^3}{3\tilde{\mu}}\rho g\tilde{\nabla}\tilde{h}\right] - \tilde{E} \tag{7}$$

The resin concentration is assumed to be uniform across the thin dimension. This "well-mixed" approximation is valid for sufficiently thin coating layers.[8] Therefore, the resin flux changes due to diffusion and convection of resin in the mixture parallel to the substrate

$$\tilde{\mathbf{Q}}_r = -\tilde{D}\tilde{h}\tilde{\nabla}\tilde{c} + \tilde{\mathbf{Q}}c \tag{8}$$

where $\tilde{\mathbf{Q}}_r = \tilde{\mathbf{Q}}_r(\tilde{x},\tilde{y},\tilde{t})$ is the flux of resin. The resin is conserved, and integral mass conservation for the resin layer requires

$$\frac{\partial\tilde{h}_r}{\partial\tilde{t}} = -\tilde{\nabla}\cdot\tilde{\mathbf{Q}}_r \tag{9}$$

Defining the depth-averaged velocity as $\tilde{\mathbf{U}} = \tilde{\mathbf{Q}}/\tilde{h}$ and using the vector identity $\tilde{h}\tilde{\nabla}\tilde{c} = \tilde{\nabla}(c\tilde{h}) - c\tilde{\nabla}\tilde{h}$, the evolution equation for the resin height can be written in divergence form

$$\frac{\partial\tilde{h}_r}{\partial\tilde{t}} = \tilde{\nabla}\cdot\left[\tilde{D}\left(\tilde{\nabla}\tilde{h}_r - \frac{\tilde{\nabla}\tilde{h}}{\tilde{h}}\tilde{h}_r\right)\right] - \tilde{\nabla}\cdot(\tilde{\mathbf{U}}\tilde{h}_r) \tag{10}$$

It is also possible to derive an equation in terms of resin fraction. To this end, we can combine eqs 8 and 9 and retain the function c to get

$$\frac{\partial(c\tilde{h})}{\partial\tilde{t}} = -\tilde{\nabla}\cdot(-\tilde{D}\tilde{h}\tilde{\nabla}c + \tilde{\mathbf{Q}}c) \tag{11}$$

Using eq 6 we find that the final dimensional evolution equation for the resin fraction is

$$\frac{\partial c}{\partial\tilde{t}} = \frac{1}{\tilde{h}}\tilde{\nabla}\cdot(\tilde{D}\tilde{h}\tilde{\nabla}c) + \left(\frac{\tilde{E}}{\tilde{h}}\right)c - \tilde{\mathbf{U}}\cdot\tilde{\nabla}c \tag{12}$$

The viscosity of the coating is a strong function of resin concentration. We use an exponential form[11,12] as the viscosity model. It is given as

$$\tilde{\mu} = \tilde{\mu}^{(0)}\exp[M(c - c^{(0)})] \tag{13}$$

where M is an empirical constant, $\tilde{\mu}^{(0)}$ is the initial viscosity, and $c^{(0)}$ is the initial resin fraction. We use $M > 0$ to model the increase in viscosity as the resin concentration increases. Diffusivity may be assumed to be inversely proportional to the viscosity;[13−15] thus, we use

$$\tilde{D} = \tilde{D}^{(0)}\exp[-M(c - c^{(0)})] \tag{14}$$

where $\tilde{D}^{(0)}$ is the initial diffusivity. The surface tension is assumed to be a linear function of resin concentration[16]

$$\tilde{\sigma} = \tilde{\sigma}_s + (\tilde{\sigma}_r - \tilde{\sigma}_s)c, \tag{15}$$

where $\tilde{\sigma}_s$ and $\tilde{\sigma}_r$ are the surface tension of pure solvent and pure resin, respectively. Rather than solve the transport equations across the thin dimension, we postulate an evaporation law of the form

$$\tilde{E} = \tilde{E}^{(0)}f(\tilde{x},\tilde{y},\tilde{t})(1 - c)^n \tag{16}$$

where n is an empirical exponent to model the diminishing behavior of the evaporation rate as the resin fraction increases. The function f is dimensionless, and it takes into account spatial and temporal variations in the evaporation rate not due to resin concentration. The constant $\tilde{E}^{(0)}$ has units of velocity.

3. Nondimensionalization

The number of parameters of the problem can be reduced by nondimensionalization. We define the dimensionless independent variables as

$$x = \frac{\tilde{x}}{L}, \quad y = \frac{\tilde{y}}{L}, \quad t = \frac{\tilde{t}}{T}$$

and the dimensionless dependent variables as

$$h = \frac{\tilde{h}}{H}, \quad h_r = \frac{\tilde{h}_r}{H}, \quad \sigma = \frac{\tilde{\sigma}}{\tilde{\sigma}^{(0)}}, \quad \mu = \frac{\tilde{\mu}}{\tilde{\mu}^{(0)}},$$
$$E = \frac{T}{H}\tilde{E}, \quad \mathbf{U} = \frac{T}{L}\tilde{\mathbf{U}}, \quad D = \frac{T}{L^2}\tilde{D}$$

where L, H, and T are characteristic substrate length, coating height, and time scales, respectively, and $\tilde{\sigma}^{(0)}$ is the initial value for surface tension. Using the time scale

$$T = \frac{3\tilde{\mu}^{(0)}L^4}{\tilde{\sigma}^{(0)}H^3} \tag{17}$$

(11) Lyons, P. F.; Tobolsky, A. V. *Polym. Eng. Sci.* **1970**, *10* (1), 1.
(12) Rink, M.; Pavan, A.; Roccasalvo, S. *Polym. Eng. Sci.* **1978**, *18* (10), 755.
(13) Levich, V. G. *Physiochemical hydrodynamics*; Prentice-Hall, Inc.: New York, 1962.
(14) Flack, W. W.; Soong, D. S.; Bell, A. T.; Hess, D. W. *J. Appl. Phys.* **1984**, *56* (4), 1199.
(15) Fujita, H.; Kishimoto, A.; Matsumoto, K. *Trans. Faraday Soc.* **1960**, *56*, 424.
(16) Ober, R.; Paz, L.; Taupin, C.; Pincus, P. *Macromolecules* **1983**, *16* (1), 50.

the evolution equation for $\tilde{h}$, eq 7, becomes

$$\frac{\partial h}{\partial t} = -\nabla\cdot\left(\frac{3}{2}\frac{L^2}{H^2}\frac{h^2}{\mu}\nabla\sigma + \frac{h^3}{\mu}\nabla^2 h\nabla\sigma + \frac{\sigma h^3}{\mu}\nabla\nabla^2 h - B^{(0)}\frac{h^3}{\mu}\nabla h\right) - E \quad (18)$$

where the initial Bond number is given by

$$B^{(0)} = \frac{\rho g L^2}{\tilde{\sigma}^{(0)}} \quad (19)$$

The first term in eq 18 is of relative order L^2/H^2 greater than the second term. Limiting our analysis to thin coatings where $H/L \ll 1$, we neglect the second term. Replacing σ in favor of c, the final dimensionless evolution equation for h is given by

$$\frac{\partial h}{\partial t} = -\nabla\cdot\left(A\Gamma\frac{h^2}{\mu}\nabla c + \frac{h^3}{\mu}\sigma\nabla\nabla^2 h - B^{(0)}\frac{h^3}{\mu}\nabla h\right) - E \quad (20)$$

where the aspect ratio A is defined as

$$A = \frac{3}{2}\frac{L^2}{H^2}$$

and Γ is

$$\Gamma = \frac{\tilde{\sigma}_r - \tilde{\sigma}_s}{\tilde{\sigma}^{(0)}}$$

The evolution equation for the resin height, eq 10, written in dimensionless quantities, is

$$\frac{\partial h_r}{\partial t} = \nabla\cdot\left[D\left(\nabla h_r - \left(\frac{\nabla h}{h}h_r\right)\right)\right] - \nabla\cdot(\mathbf{U}h_r) \quad (21)$$

With a similar procedure we transform the evolution equation of the resin fraction, eq 12, into the following dimensionless form,

$$\frac{\partial c}{\partial t} = \frac{1}{h}\nabla\cdot(Dh\nabla c) + \left(\frac{E}{h}\right)c - \mathbf{U}\cdot\nabla c \quad (22)$$

The dimensionless forms of viscosity, diffusivity, surface tension, and evaporation rate are

$$\mu = \exp[M(c - c^{(0)})] \quad (23)$$

$$D = \frac{T}{L^2}\tilde{D}^{(0)}\exp[-M(c - c^{(0)})] = D^{(0)}\exp[-M(c - c^{(0)})]$$

$$\sigma = \frac{\tilde{\sigma}_s + (\tilde{\sigma}_r - \tilde{\sigma}_s)c}{\tilde{\sigma}^{(0)}}$$

and

$$E = \frac{T}{H}\tilde{E}^{(0)}f(\tilde{x},\tilde{y},\tilde{t})(1 - c)^n = E^{(0)}f(x,y,t)(1 - c)^n \quad (24)$$

A total of six dimensionless parameters characterize the coating liquid:

1. $A\Gamma$—The of effect of surface tension gradients on the flow. Because A and Γ are always found together, they represent one dimensionless parameter.

2. $B^{(0)}$—The Bond number is the ratio of gravity to surface tension effect in leveling the surface. It includes the length scale L and so is a function of the geometry of the film.

3. $E^{(0)}$—The dimensionless evaporation rate measures the effect of solvent evaporation. This term affects $\partial h/\partial t$ directly through eq 18 and indirectly due to its effect on the resin concentration.

4. $D^{(0)}$—The dimensionless diffusion rate measures the effect of lateral diffusion of resin in the bulk liquid.

5. M—The exponent in the viscosity−concentration and diffusion−concentration formulas.

6. n—This dimensionless factor measures the effect of resin concentration on evaporation. When $n = 0$ the rate-controlling mechanism for evaporation is a change of phase at the interface leading to a constant evaporation rate. For $0 \le n \le 1$, the evaporation rate is a function of resin concentration.

For a starting profile given by

$$\tilde{h}(\tilde{x},\tilde{y},\tilde{t} = 0) = \tilde{h}^{(0)} + \tilde{a}^{(0)}\cos(2\pi\tilde{x}/\tilde{\lambda}_{\tilde{x}})\cos(2\pi\tilde{y}/\tilde{\lambda}_{\tilde{y}}) \quad (25)$$

where $\tilde{h}^{(0)}$ is the initial average coating height, $\tilde{a}^{(0)}$ is the initial amplitude of the profile, and $(\tilde{\lambda}_{\tilde{x}}, \tilde{\lambda}_{\tilde{y}})$ are the wavelengths in the $\tilde{x}$ and $\tilde{y}$ directions, we use a characteristic substrate length L given by $\tilde{\lambda}_{\tilde{x}}/2$ and a characteristic coating height H given by $\tilde{h}^{(0)}$. Hence, we have two additional dimensionless parameters characterizing the initial conditions:

1. $a^{(0)} = \tilde{a}^{(0)}/H$—The dimensionless starting amplitude.

2. $\lambda_y = \tilde{\lambda}_{\tilde{y}}/L = 2\tilde{\lambda}_{\tilde{y}}/\tilde{\lambda}_{\tilde{x}}$—The initial dimensionless wavelength in the y direction (or twice the ratio of wavelengths in x and y directions for this length scale L)

4. Linearized Theory

It is possible to linearize eqs 20 and 22 by assuming that the coating height, resin fraction, and surface tension differ only slightly from their initial values. Furthermore, we assume that the viscosity, diffusivity, and evaporation rate are constant in time. The dimensionless evolution equations for the coating height and resin concentration simplify to

$$\frac{\partial h}{\partial t} = -\nabla\cdot(A\Gamma h^2\nabla c + h^3\sigma\nabla\nabla^2 h - B^{(0)}h^3\nabla h) - E^{(0)} \quad (26)$$

and

$$\frac{\partial c}{\partial t} = D\left(\nabla^2 c + \frac{\nabla h}{h}\cdot\nabla c\right) + \left(\frac{E}{h}\right)c - \mathbf{U}\cdot\nabla c \quad (27)$$

For the initial conditions we use the dimensionless form of eq 25 and assume uniform resin concentration and surface tension

$$h(x,y,t = 0) = 1 + \epsilon\cos(k_x x)\cos(k_y y)$$

$$c(x,y,t = 0) = c^{(0)}$$

$$\sigma(x,y,t = 0) = 1 \quad (28)$$

where $\epsilon \equiv a^{(0)}$ and (k_x, k_y) are the dimensionless wavenumbers in the x and y directions: $k_x = 2\pi/\lambda_x$ and $k_y = 2\pi/\lambda_y$. Since $\epsilon \ll 1$, the dependent variables differ only

slightly from their starting values, and they can be expanded in power series

$$h(x,y,t) = h_0(t) + \epsilon h_1(x,y,t) + O(\epsilon^2)$$

$$c(x,y,t) = c_0(t) + \epsilon c_1(x,y,t) + O(\epsilon^2)$$

$$\sigma(x,y,t) = \sigma_0(t) + \epsilon \sigma_1(x,y,t) + O(\epsilon^2) \quad (29)$$

The $O(\epsilon^0)$ equations are

$$\frac{\partial h_0}{\partial t} = -E^{(0)}$$

$$\frac{\partial c_0}{\partial t} = E^{(0)}\frac{c_0}{h_0} \quad (30)$$

Integrating and using the $O(\epsilon^0)$ initial conditions, we obtain

$$h_0(t) = 1 - E^{(0)}t$$

$$c_0(t) = \frac{c^{(0)}}{1 - E^{(0)}t} \quad (31)$$

Here, $h_0(t)$ and $c_0(t)$ describe a uniform coating layer evaporating at a constant rate, and the consequent increase in resin concentration. We further assume that the term $E^{(0)}t$ is $O(\epsilon)$. The $O(\epsilon)$ system is

$$\frac{\partial h_1}{\partial t} = -A\Gamma\nabla^2 c_1 - \nabla^4 h_1 + B^{(0)}\nabla^2 h_1$$

$$\frac{\partial c_1}{\partial t} = D\nabla^2 c_1 + E^{(0)}c^{(0)}\left(\frac{c_1}{c^{(0)}} - h_1\right) \quad (32)$$

We seek a separable solution of the form

$$h_1(x,y,t) = \alpha(t)\cos(k_x x)\cos(k_y y)$$

$$c_1(x,y,t) = \beta(t)\cos(k_x x)\cos(k_y y) \quad (33)$$

Inserting eq 33 in eq 32 and defining the effective wavenumber as $K^2 = k_x^2 + k_y^2$ yields two coupled linear ordinary differential equations

$$\frac{d\alpha}{dt} = -(K^4 + B^{(0)}K^2)\alpha + A\Gamma K^2\beta$$

$$\frac{d\beta}{dt} = -E^{(0)}c^{(0)}\alpha + (E^{(0)} - DK^2)\beta \quad (34)$$

with initial conditions $\alpha(0) = 1$ and $\beta(0) = 0$. If

$$[E^{(0)} - (B^{(0)} + D)K^2 - K^4]^2 - 4[A\Gamma E^{(0)}c^{(0)}K^2 - (K^4 + B^{(0)}K^2)(E^{(0)} - DK^2)] > 0 \quad (35)$$

the eigenvalues of eq 34 are real and the solutions for $\alpha(t)$ and $\beta(t)$ are

$$\alpha(t) = C_1 e^{\lambda_1 t} + C_2 e^{\lambda_2 t}$$

$$\beta(t) = \frac{1}{A\Gamma K^2}[C_1(\lambda_1 + B^{(0)}K^2 + K^4)e^{\lambda_1 t} + C_2(\lambda_2 + B^{(0)}K^2 + K^4)e^{\lambda_2 t}] \quad (35)$$

where

$$C_1 = -\frac{\lambda_2 + B^{(0)}K^2 + K^4}{\lambda_1 - \lambda_2}$$

$$C_2 = 1 + \frac{\lambda_2 + B^{(0)}K^2 + K^4}{\lambda_1 - \lambda_2}$$

$$\lambda_{1,2} = \frac{E^{(0)} - (B^{(0)} + D)K^2 - K^4}{2} \pm \frac{1}{2}([E^{(0)} - (B^{(0)} + D)K^2 - K^4]^2 - 4[A\Gamma E^{(0)}c^{(0)}K^2 - (K^4 + B^{(0)}K^2)(E^{(0)} - DK^2)])^{1/2}$$

This solution represents an exponential change in amplitudes without any "rebound" effect. When the left side of eq 35 is negative, the eigenvalues are complex, and the solutions for $\alpha(t)$ and $\beta(t)$ are

$$\alpha(t) = e^{\omega_R t}\left[\cos\omega_I t - \frac{\omega_R + B^{(0)}K^2 + K^4}{\omega_I}\sin\omega_I t\right]$$

$$\beta(t) = -\frac{e^{\omega_R t}}{\omega_I A\Gamma K^2}[(\omega_R + B^{(0)}K^2 + K^4)^2 + \omega_I^2]\sin\omega_I t \quad (37)$$

where

$$\omega_R = \frac{E^{(0)} - (B^{(0)} + D)K^2 - K^4}{2}$$

$$\omega_I = \frac{1}{2}(4[A\Gamma E^{(0)}c^{(0)}K^2 - (K^4 + B^{(0)}K^2)(E^{(0)} - DK^2)] - [E^{(0)} - (B^{(0)} + D)K^2 - K^4]^2)^{1/2}$$

At $x = y = 0$ the perturbation solution up to $O(\epsilon)$ is

$$h(t) = (1 - E^{(0)}t) + \epsilon e^{\omega_R t}\left[\cos\omega_I t - \frac{\omega_R + B^{(0)}K^2 + K^4}{\omega_I}\sin\omega_I t\right] + O(\epsilon^2) \quad (38)$$

$$c(t) = \frac{c^{(0)}}{1 - E^{(0)}t} - \epsilon\frac{e^{\omega_R t}}{\omega_I A\Gamma K^2}[(\omega_R + B^{(0)}K^2 + K^4)^2 + \omega_I^2]\sin\omega_I t + O(\epsilon^2) \quad (39)$$

This approximate solution will be compared with the full numerical solution below.

5. Numerical Implementation

In order to solve the evolution equations for h and h_r numerically, we discretize the flow domain and approximate the partial derivatives using finite differences. A purely explicit numerical time integration for the coating and resin heights, where the "new" values of the dependent variables are found using only "old" values, is the most straightforward finite difference implementation of the governing partial differential equations. Unfortunately, such a scheme requires a very small time step for stability and consequently is computationally inefficient. An implicit time-marching method for finding the new values of h and h_r eliminates this time step limitation but introduces another difficulty; at each time step a very large coupled system must be inverted. The method of alternating directions, proposed by Peaceman and Rach-

ford[17] and Douglas[18] to solve the two-dimensional heat equation, avoids these two limitations. In this scheme the x-derivatives are treated implicitly and y-derivatives explicitly for the first half time step, and the y-derivatives are treated implicitly and x-derivatives explicitly in the second half time step. This method is unconditionally stable and, for the heat equation, requires the solution of a tridiagonal system of equations at each half time step. Unfortunately this scheme is no longer unconditionally stable when used with higher order equations such as the biharmonic equation. A method termed the "stabilizing correction scheme" was used by Conte[19] and Conte and Dames[20,21] to solve the biharmonic equation. This scheme is unconditionally stable and provides a promising option for the elimination of time step limitations. Another effective scheme for the numerical solution of the biharmonic equation was proposed by Yanenko[22] and is termed the "time-splitting scheme."

Equations 20 and 21 are solved with a partially implicit time-splitting scheme. The time integration is partially-implicit in the sense that both the nonlinear prefactors h^2 and h^3 and the mixed derivative terms are evaluated at the previous time level. In the x-sweep the x-component of eq 20 is considered, and intermediate values of h are found by solving a pentadiagonal system of equations. The x-component of the average velocity vector is found by numerical integration. Intermediate values of h_r are found by solving a tridiagonal system of equations arising from the x-component of equation eq 20. In the y-sweep, which is symmetric to the x-sweep, the y-components of eqs 20 and 21 are solved. Finally, viscosity, diffusivity, surface tension, and evaporation rate values are updated at the end of the time step.

6. Results and Discussion

In this section we first examine results from the linear solution presented in section 4 to help explain the interaction between the coating height h and the resin concentration c. In section 6.1 the linear results are compared with those from nonlinear numerical simulations, obtained using the partially implicit time-splitting method outlined in section 5. We explain differences between the results from the two solution methods, and use the similarities in the linear regime to help verify our numerical implementation. In section 6.2 we show a sample simulation of the full nonlinear problem, using parameters characteristic of a typical solvent-based alkyd paint. We will use several different plots to illustrate and explain the complex evolution of the coating height $h(x,y,t)$, and the resin concentration $c(x,y,t)$, during the drying-leveling process. In section 6.3, we examine the effects of three dimensionless parameters characterizing the liquid, Γ, $E^{(0)}$, and λ_y, and show the dependence of the final coating height variation on these parameters. In section 6.4 we consider the effect of spatial evaporation gradients and conclude with a summary of our results.

6.1. Results from Linear Theory. Figure 2 shows the time evolution of the coating height at the initial crest, $h(0,0,t)$, for various values of the dimensionless starting amplitude ϵ in eq 38. The initial profile is given by eq 28 with $k_x = k_y = \pi$. The dimensionless parameters for this simulation are given in Table 2. The nonlinear solution was obtained by solving the coupled system of partial differential eqs 20 and 21 numerically by using the partially implicit time-splitting scheme. In the nonlinear simulation, the increase in viscosity and the change in resin diffusivity with resin concentration are ignored, so the difference between the linear and nonlinear results is expected to come only from the h^2 and h^3 prefactors in front of the flux terms in eq 20.

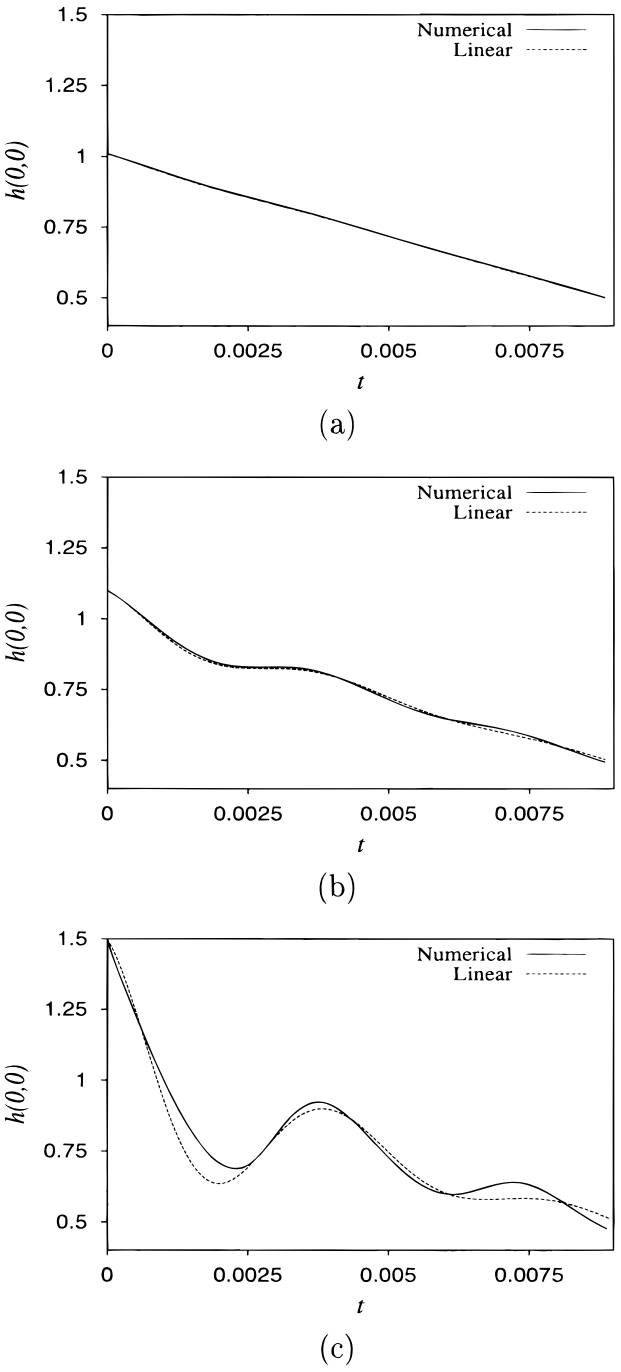

Figure 2. Comparison of numerical and linearized solutions of $h(0,0,t)$ for different values of the initial amplitude ϵ: (a) $\epsilon = 0.01$; (b) $\epsilon = 0.1$; (c) $\epsilon = 0.5$.

For all of the cases shown in Figure 2, $h(0,0,t)$ oscillates in time, while gradually decreasing due to solvent evaporation. For a small initial amplitude ϵ, shown in Figure 2a, the effect of resin concentration gradients (and therefore surface tension gradients) is small and the coating layer levels with an almost constant rate of $\partial h/\partial t$

(17) Peaceman, D. W.; Rachford, H. H., Jr. *SIAM J.* **1955**, *3*, 28.
(18) Douglas, J., Jr. *SIAM J.* **1955**, *3*, 42.
(19) Conte, S. D. *Pac. J. Math.* **1957**, *7*, 1535.
(20) Conte, S. D.; Dames, R. T. *Math. Tables Aids Comput.* **1958**, *12*, 198.
(21) Conte, S. D.; Dames, R. T. *ACM J.* **1960**, *7*, 264.
(22) Yanenko, N. N. *The method of fractional steps*; Springer-Verlag: New York, 1971.

$= -E^{(0)} = -56$. For larger ϵ, shown in Figure 2b and c, the magnitude of the oscillations, for both the linear and nonlinear solutions, grows with increasing ϵ. For the linear solution, this increase in amplitude is clearly due to the ϵ term multiplying the sinusoidal term in the second term of eq 38. Physically, the effect of increasing the initial amplitude is to cause a larger spatial resin concentration gradient between the initial trough regions and the initial crests. The larger the resin concentration gradients, the larger the surface tension gradients which act to drive liquid from the crests to the troughs. These surface tension gradients initially act to encourage leveling. But the resin concentration gradients remain after the surface is perfectly level. Due to the continued action of these surface tension gradient forces, the coating height at the corner falls below $h(0,0,t) = 1 - E^{(0)}t$, reaching a minimum at $t \approx 0.002$. For subsequent times, $h(0,0,t)$ goes through a series of maximums and minimums while gradually lowering due to solvent evaporation, as shown in Figures 2b and c.

These oscillations in $h(0,0,t)$ are driven by resin concentration gradients, which are in turn driven by coating height gradients. Because spatial differences in h and c drive the flow, this interplay between h and c is best understood by examining the difference in h and c values between the initial crests and initial troughs. From the linear solution, we find

$$\Delta h(t) = h(0,0,t) - h(1,0,t)$$

$$= 2\epsilon e^{\omega_R t}\left[\cos \omega_I t - \frac{\omega_R + B^{(0)}K^2 + K^4}{\omega_I} \sin \omega_I t\right] + O(\epsilon^2) \quad (40)$$

$$\Delta c(t) = c(0,0,t) - c(1,0,t)$$

$$= -2\epsilon \frac{e^{\omega_R t}}{\omega_I A\Gamma K^2}[(\omega_R + B^{(0)}K^2 + K^4)^2 + \omega_I{}^2] \sin \omega_I t + O(\epsilon^2) \quad (41)$$

Figure 3 shows a plot of $\Delta h(t)$ and $\Delta c(t)$ for the same parameters considered in Figure 2b. When $\Delta c(t)$ is negative, the surface tension at ($x = 0$, $y = 0$) is less than that at ($x = 1$, $y = 0$), and surface tension gradients cause a net flow from ($x = 0$, $y = 0$) to ($x = 1$, $y = 0$). If $\Delta h(t)$ is positive when $\Delta c(t)$ is negative, this flow will encourage leveling. If $\Delta h(t)$ is negative when $\Delta c(t)$ is negative, this flow will cause deleveling. When $\Delta c(t)$ is positive, a negative $\Delta h(t)$ will encourage leveling and a positive $\Delta h(t)$ deleveling. On the other hand, surface tension and gravitational forces always encourage leveling. For the case shown in Figure 3, surface tension gradients promote leveling for the times $0 < t < 0.001$, $0.0021 < t < 0.0031$, and $0.0042 < t < 0.0052$, and cause deleveling for the times $0.001 < t < 0.0021$, $0.0031 < t < 0.0042$, and $0.0052 < t < 0.0064$.

Note that the first minimum of $\Delta h(t)$ at $t = 0.002$ in Figure 3 occurs slightly before $\Delta c(t)$ is exactly zero at $t = 0.0021$. This is due to the leveling effect of gravitational and surface tension forces, which act against surface tension gradient forces during the time frame $0.001 \le t \le 0.0021$ but are only strong enough to counter the deleveling effects of surface tension gradients when $\Delta c(t)$ is very close to zero. The same phenomenon causes the time lag between subsequent maximums and minimums in $\Delta h(t)$ and the zeros in $\Delta c(t)$, as shown in Figure 3. For

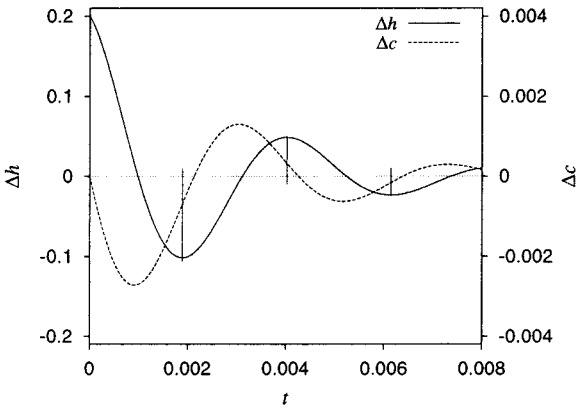

Figure 3. Difference in coating height between the initial crests and the initial troughs $\Delta h(t) = h(0,0,t) - h(1,0,t)$ as a function of time for the linear solution, plotted with the difference in resin concentration between these two regions $\Delta c(t) = c(0,0,t) - c(1,0,t)$. Here $\epsilon = 0.1$.

this simulation, the values used correspond to

$$A\Gamma \gg 1, \quad B^{(0)} \sim O(1), \quad K \sim O(1)$$

yielding

$$\omega_I \gg (\omega_R + B^{(0)}K^2 + K^4)$$

and the cosine term in eq 40 is much larger than the sine term. In this regime, surface tension gradients drive the flow; thus

$$\Delta h(t) \sim e^{\omega_R t} \cos(\omega_I t)$$

$$\Delta c(t) \sim e^{\omega_R t} \cos(\pi/2 + \omega_I t)$$

and $\Delta h(t)$ and $\Delta c(t)$ are exponentially decaying sinusoids that are out of phase by $\pi/(2\omega_I)$ dimensionless time units.

Returning to Figure 2, we note that the difference between the nonlinear solution and the linear solution grows with increasing ϵ. This is expected because the h^2 and h^3 prefactors in eq 20 cause a discrepancy in the fluxes between the linear and nonlinear solutions. At the crests, where $h > 1$, the fluxes are greater for the nonlinear solution compared to the linear solution; at the troughs, where $h < 1$, the fluxes are greater in the linear solution. Examining the $\epsilon = 0.5$ case in Figure 2c, we see that for very early times, $t < 0.0003$, the magnitude of the leveling rate $|\partial h/\partial t|$ is greater for the nonlinear solution. During this period, $h(x,y,t) > 1$ in the region near ($x = 0$, $y = 0$) and the nonlinear prefactors amplify the net flux away from this region. But in trough regions near ($x = 1$, $y = 0$), $h(x,y,t) < 1$ and the nonlinear prefactors slow the net flux into these regions. Because $h(0,0,t)$ is a function of how fast the liquid can drain from the crest into the trough region, the net effect of the nonlinear prefactors is to decrease $|\partial h/\partial t|$ in the nonlinear solution for $0.0003 < t < 0.002$. As a result of this difference, $h(0,0,t)$ reaches a lower initial minimum at an earlier time for the linear solution in Figure 2c. Subsequent discrepancies between the linear and nonlinear solutions are more difficult to analyze due to the complex interaction between evaporation and the spatial h and c gradients.

6.2. Model Simulations. In this section we use computer simulations, based on the theory and numerical algorithm developed in sections 2−5, to model the leveling behavior of a typical solvent-based alkyd paint. Specifically, we consider the leveling history of two different

Table 1. Physical Properties and Initial Conditions for Our Model Simulations

parameter	symbol	value(2D)	value(3D)	units (cgs)
surface tension of solvent	$\tilde{\sigma}_s$	23.375	23.0	dyn/cm
surface tension of resin	$\tilde{\sigma}_r$	30.875	30.0	dyn/cm
initial surface tension of the coating	$\tilde{\sigma}^{(0)}$	27.5	26.5	dyn/cm
initial viscosity	$\tilde{\mu}^{(0)}$	15.9	5.0	g/(cm s)
initial diffusivity	$\tilde{D}^{(0)}$	1.0×10^{-5}	1.0×10^{-5}	cm^2/s
density	ρ	0.77	0.75	g/cm^3
initial evaporation rate	$\tilde{E}^{(0)}$	0.2×10^{-6}	1.0×10^{-6}	cm/s
initial resin fraction	$c^{(0)}$	0.55	0.5	
evaporation−concentration exponent	n	1.0	0.5	
viscosity−concentration exponent diffusion−concentration exponent	M	15.0	15.0	
average coating height	$\tilde{h}^{(0)}$	0.0056	0.005	cm
initial amplitude	$\tilde{a}^{(0)}$	0.0025	0.0025	cm
wavelength in $\tilde{x}$ direction	$\tilde{\lambda}_{\tilde{x}}$	0.4	1.0	cm
wavelength in $\tilde{y}$ direction	$\tilde{\lambda}_{\tilde{y}}$		1.0	cm

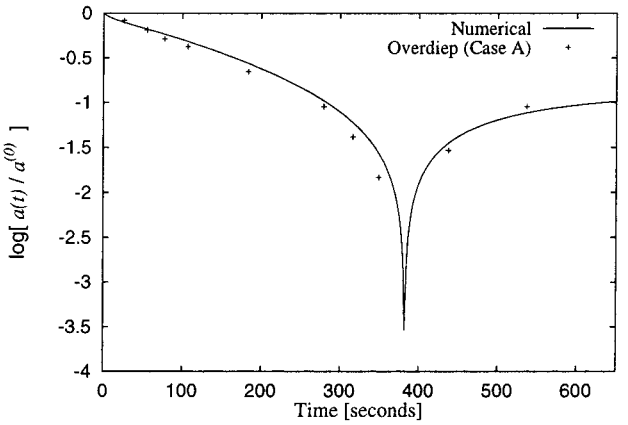

Figure 4. Evolution of the wave amplitude for a two-dimensional coating. Here, $a(t)$ is the dimensionless amplitude of the wave, and $a^{(0)}$ is the dimensionless initial amplitude. The physical parameters are listed in Table 1. The solid line is the two-dimensional numerical simulation. The experimental data points are extracted from ref 2.

Table 2. Dimensionless Parameters for Our Three-Dimensional Model Coating Simulation[a]

symbol	definition	value
A	$^3/_2(L^2/H^2)$	1.5×10^4
Γ	$(\tilde{\sigma}_r - \tilde{\sigma}_s)/\tilde{\sigma}^{(0)}$	0.26
$B^{(0)}$	$\rho g L^2/\tilde{\sigma}^{(0)}$	6.9
$D^{(0)}$	$\tilde{D}^{(0)}T/L^2$	11.0
$E^{(0)}$	$\tilde{E}^{(0)}T/H$	56.0
k_x	$2\pi L/\tilde{\lambda}_{\tilde{x}}$	π
k_y	$2\pi L/\tilde{\lambda}_{\tilde{y}}$	π
$a^{(0)}$	$\tilde{a}^{(0)}/H$	0.5

[a] The length scale along the substrate L is taken to be $L = \tilde{\lambda}_{\tilde{x}}/2 = 0.5$ cm; the length scale perpendicular to the substrate is taken to be $H = 0.005$ cm; and the time scale is $T = 2.8 \times 10^5$ using eq 17.

paints with the physical parameters listed in Table 1. The physiochemical properties of our model paints were chosen to be similar to the ones considered by Overdiep[2] in his study of the two-dimensional leveling behavior of alkyd paints.

Overdiep used a doctor blade to generate two-dimensional square waves with known wavelengths and amplitudes. The surface wave amplitude is then recorded and measured in time. In his work, Overdiep presented the evolution of the normalized amplitude for two different alkyd paints. In Figure 4 we show a comparison between Overdiep's Case A experiment and the two-dimensional (2D) numerical simulation. The physical parameters for the 2D simulation are given in Table 1.

For our three-dimensional model simulation the initial profile is given by equation 25, where values for H, $\tilde{a}^{(0)}$, $\tilde{\lambda}_{\tilde{x}}$, and $\tilde{\lambda}_{\tilde{y}}$ are given in Table 1. The values for the dimensionless parameters for this simulation are listed in Table 2. Due to symmetry, we may consider only the domain ($0 \le \tilde{x} \le \tilde{\lambda}_{\tilde{x}}/2$; $0 \le \tilde{y} \le \tilde{\lambda}_{\tilde{y}}/2$), corresponding to ($0 \le x \le 1$; $0 \le y \le 1$) in dimensionless units, and impose zero-slope, zero-flux boundary conditions at the computational boundaries.

Figure 5 shows three-dimensional views of both the dimensionless coating height $h(x,y)$ and the resin concentration $c(x,y)$ for six different output times during the drying−leveling process of our model coating. The initial coating height and resin concentration profiles are shown in Figure 5a. At this initial time, the resin concentration is uniform and the coating height has two crests in the approximate regions ($x < 0.25$, $y < 0.25$) and ($x > 0.75$, $y > 0.75$) and two shallow troughs in the approximate regions ($x > 0.75$, $y < 0.25$) and ($x < 0.25$, $y > 0.75$). Examination of eq 20 shows that h changes due to four distinct mechanisms: (i) flux due to surface tension gradient effects [$Q_{stg} = A\Gamma(h^2/\mu)\nabla c$], (ii) flux due to surface tension effects [$Q_{st} = \sigma(h^3/\mu)\nabla\nabla^2 h$], (iii) flux due to gravitational effects [$Q_g = -B^{(0)}(h^3/\mu)\nabla h$], and (iv) a decrease in h due to solvent evaporation E. Initially the flow is driven mainly by Q_{st} and Q_g, both of which act to level the uneven surface, while evaporation steadily lowers the average value of the coating height. But the increase in resin concentration due to solvent evaporation is not uniform; according to the second term in eq 22, evaporation causes resin concentration increases at a rate that is inversely proportional to the coating height. Thus, the resin concentration increases at a faster rate in the troughs relative to the crests, causing a flux Q_{stg} which acts to move liquid from thick regions to thin regions, enhancing the leveling effect of Q_{st} and Q_g.

Figure 6 shows a plot of the maximum value of each of these three fluxes in the flow field as a function of time. Several distinct flow regimes are clearly indicated. In the first region, $0 < t < 0.001$, Q_{st} and Q_g gradually decrease as the surface levels, while Q_{stg} increases due to a continued increase in the difference in resin concentration, and surface tension, between the crests and the troughs. This is illustrated in Figure 5b. Here the coating height is similar in shape to the original profile shown in Figure 5a, but the profile is much flatter: the difference between the maximum and minimum values for the coating height in Figure 5a is unity compared to the difference in the maximum and minimum values for the coating height in Figure 5b of 0.24. Because both Q_{st} and Q_g depend on the gradients of the coating height, the maximum values in these fluxes have been reduced by a factor of approximately 4 from their initial values, as shown in Figure 6. Figure

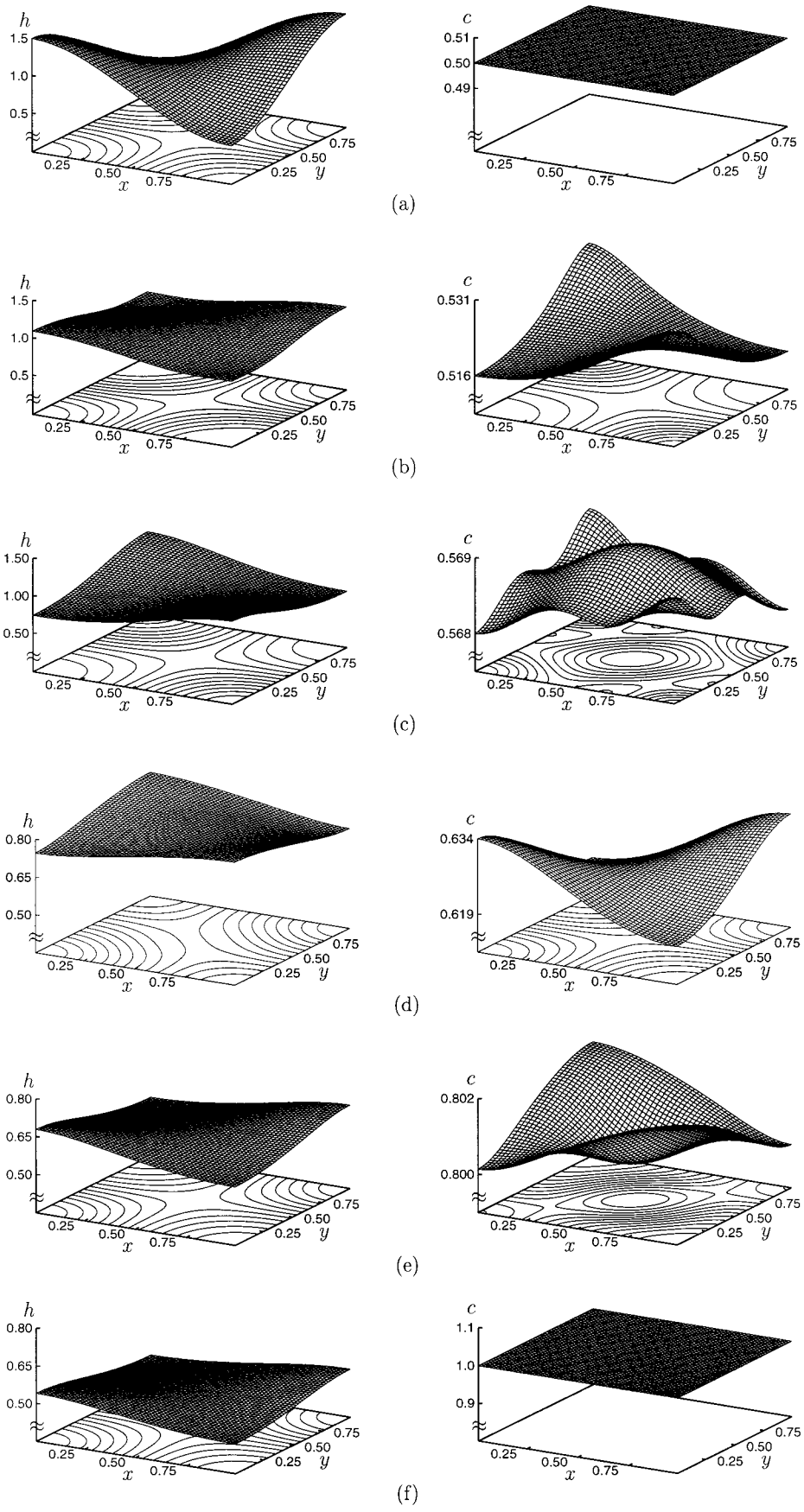

Figure 5. Time evolution of coating height and resin concentration for our example case. The physical parameters are listed in Table 1. (a) $t = 0$; (b) $t = 0.001$; (c) $t = 0.0031$; (d) $t = 0.0054$; (e) $t = 0.011$; and (f) $t = 0.0198$. The numbers on the z axis for the resin concentration plots in parts b and e represent the maximum and minimum values for resin concentration at each time. Note that both the h and c plots are symmetric about the lines $y = x$ and $y = 1 - x$.

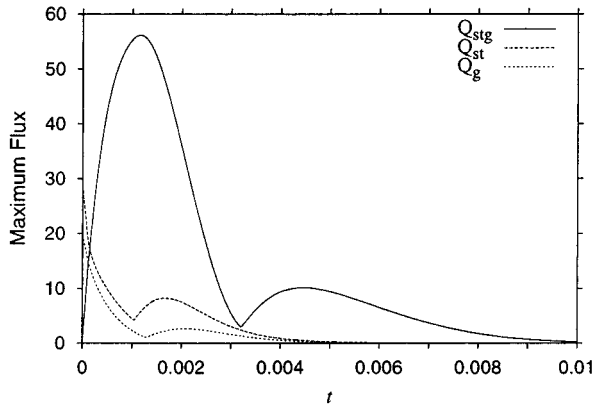

Figure 6. Maximum value of the fluxes due to (i) surface tension gradients, Q_{stg}, (ii) surface tension, Q_{st}, and (iii) gravity, Q_g, as a function of time for our model coating during the drying−leveling process. The general decrease in the magnitude of the fluxes is due primarily to the large increase in viscosity as the solvent evaporates.

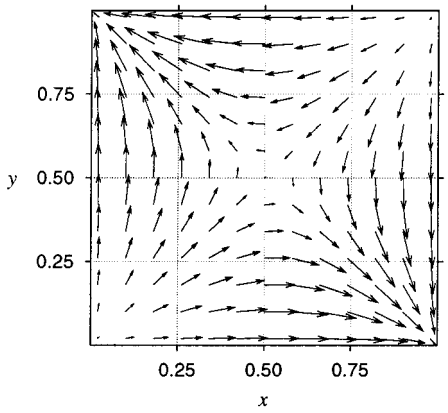

Figure 7. Flux vector field immediately before the start of the first reversal in the coating height at $t = 0.001$. At this time the fluxes act to draw liquid away from the crests toward the troughs, as shown in the coating height plot in Figure 5b.

5b shows that the resin concentration is indeed higher in regions which were initially troughs in the coating height, and lower at the crests. Note that the difference between the maximum and minimum values for resin concentration is only 0.015. Despite the small magnitudes in resin concentration gradients, the Q_{stg} term is much larger than Q_{st} and Q_g due to the thinness of the coating layer. As a result of the continued action of these surface tension gradients, the coating height undergoes a "reversal" starting at $t \approx 0.001$. The flux vector field immediately before the start of the first reversal is shown in Figure 7.

Once the coating height has undergone a reversal, the resin concentration increases at a faster rate in regions which are now troughs [in the approximate regions ($x < 0.25, y < 0.25$) and ($x > 0.75, y > 0.75$)] compared to regions which are now crests [in the approximate regions ($x > 0.75, y < 0.25$) and ($x < 0.25, y > 0.75$)], but the flux due to surface tension gradients continues to drive liquid toward the "new" crests and away from the "new" troughs, countering the leveling effect due to Q_{st} and Q_g. But, as illustrated for $0.001 < t < 0.003$ in Figure 6, the maximum values for Q_{stg} are much larger than those for Q_{st} and Q_g, causing the coating height to continue to delevel. At $t = 0.0031$ the difference between the maximum and minimum values of the coating height has increased to 0.36, as shown in Figure 5c. At $t \approx 0.0031$, the resin concentration undergoes a reversal, as shown in Figure 5c. From $t = 0.0031$ to $t = 0.0057$, the fluxes from Q_{stg}, as well as Q_{st} and Q_g, act to level the coating height, causing a second reversal at $t \approx 0.0060$. From $t = 0.0057$ to $t = 0.011$, the surface tension gradients continue to drive the flow, now deleveling the coating height, until a second reversal in the resin concentration takes place at $t \approx 0.011$, as shown in Figure 5e. For $t > 0.011$, Q_{stg}, as well as Q_{st}, and Q_g, acts to level the coating height, but at these later times, $c > 0.8, \mu > 90.0$, and these fluxes are comparatively weak. During this later stage of coating evolution, the viscosity is too high to allow for significant lateral liquid movement, and the coating height primarily lowers due to evaporation of solvent until the final "dry" stage is reached. This is shown in Figure 5f.

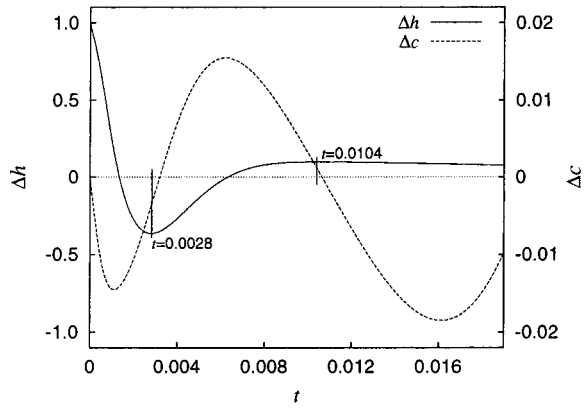

Figure 8. Difference in coating height between the initial crests and the initial troughs $\Delta h(t) = h(0,0,t) - h(1,0,t)$ as a function of time for the full nonlinear simulation, plotted with the difference in resin concentration between these two regions $\Delta c(t) = c(0,0,t) - c(1,0,t)$. The times at which $\Delta h(t)$ goes through a maximum and minimum are also labeled and shown to almost correspond to times when $\Delta c(t) = 0$. Three-dimensional plots of $c(x,y)$ during its reversals at $t = 0.0031$ and $t = 0.011$ are shown in parts c and e of Figure 5, respectively.

Figure 8 shows a plot of $\Delta h(t)$ and $\Delta c(t)$ for the same simulation. Qualitatively, the results are similar to those shown in Figure 3 for the linear solution, but with the time scale stretched due to the increase in viscosity. As in the linear solution, we find that the $\Delta h(t)$ and $\Delta c(t)$ curves are shaped like out-of-phase sinusoids and that, due to the leveling effects of Q_{st} and Q_g, the maximum and minimum values in $\Delta h(t)$ occur shortly before the $\Delta c(t)$ curve passes through zero.

6.3. Effect of Dimensionless Parameters on the Coating Evolution. In this section we investigate the effects of three of the primary dimensionless parameters characterizing the coating liquid for the problem considered in section 6. Specifically we examine the time history of the coating height $h(0,0,t)$ for varying Γ, $E^{(0)}$, and λ_y. We define the value of the difference in coating height between initial crests and troughs at the drying time t_f as

$$\Delta h_f \equiv \Delta h(t_f) = h(0,0,t_f) - h(1,0,t_f)$$

and we use Δh_f as a measure of the leveling of the coating height. The remaining parameters are left unchanged in each simulation and are listed in Tables 1 and 2.

Figure 9 shows a plot of $h(0,0,t)$ for five different values of Γ. Because the dimensionless parameter $A\Gamma$ multiplies the resin concentration gradient term in eq 20 and A is fixed at $A = 1.5 \times 10^4$ for this simulation, the effect of increasing Γ is to increase surface tension gradient effects. For the $\Gamma = 0$ case shown in Figure 9, the amplitude of the initial crest steadily decreases in time. For this case, only Q_{st} and Q_g drive the flow, and as these fluxes are proportional to spatial gradients in coating height and

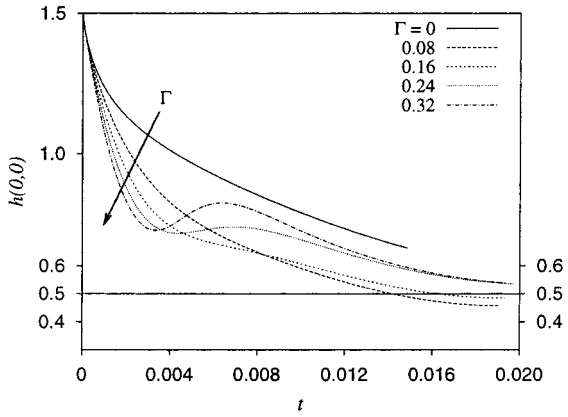

Figure 9. Coating height at the corner $h(0,0)$ as a function of time for various values of the dimensionless surface-tension-difference parameter Γ. Other dimensionless parameters are fixed and are given in Table 2. Each curve stops when all of the solvent has evaporated.

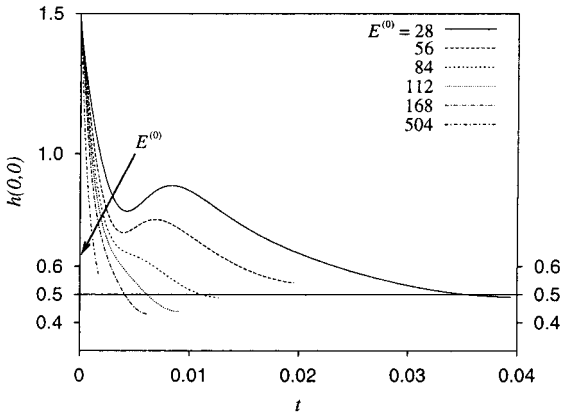

Figure 11. Coating height at the corner $h(0,0)$ as a function of time for various values of the dimensionless evaporation rate $E^{(0)}$. Other dimensionless parameters are fixed and are given in Table 2. Each curve stops when all of the solvent has evaporated.

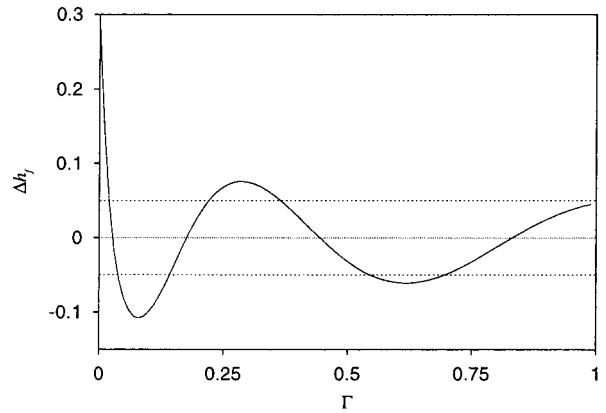

Figure 10. Difference in coating height between initial crests and initial troughs at the dry time Δh_f plotted versus Γ. Other dimensionless parameters are fixed and are given in Table 2. Also shown are the lines $\Delta h_f = -0.05$ and $\Delta h_f = 0.05$.

inversely proportional to the viscosity (which steadily increases due to solvent evaporation), the magnitude of the rate of change of the curve $h(0,0,t)$ decreases with time. The fluxes are not strong enough to cause substantial leveling before solvent evaporation freezes the coating at $h(0,0,t_f) = 0.66$. As Γ is increased, the magnitude of the rate of change of $h(0,0,t)$ increases in the early time periods, as surface tension gradient forces act with Q_{st} and Q_g to level the coating height. For the $\Gamma = 0.08$ and $\Gamma = 0.16$ cases, the coating height undergoes one reversal, yielding a negative Δh_f. For the $\Gamma = 0.24$ and $\Gamma = 0.32$ cases, the coating height undergoes two reversals, yielding a positive Δh_f.

If it is possible to adjust Γ for fixed values of the other dimensionless parameters, these results indicate that there are several distinct ranges in Γ for an optimal Δh_f. In Figure 10, we plot Δh_f as a function of Γ. If we require $|\Delta h_f| \leq 0.05$, then Γ must be within the ranges $0.019 \leq \Gamma \leq 0.038$ (in which case the coating height will undergo at most one reversal) or $0.14 \leq \Gamma \leq 0.22$ (one or two reversals) or $0.36 \leq \Gamma \leq 0.55$ (between two and three reversals) or $\Gamma \geq 0.70$ (three or more reversals). As in the linear solution, $\Delta h(t)$ takes the form of a damped sinusoid and the amplitude of each successive oscillation in $\Delta h(t)$ decreases with each coating height reversal. Consequently the permissible range of Γ for a given maximum $|\Delta h_f|$ increases with an increasing number of coating height reversals. Note that even when Γ is very small, surface tension gradients may cause significant leveling. For example, when $\Gamma = 0.02$, corresponding to a difference in surface tension between the resin and the solvent of only 2%, the final $\Delta h_f = 0.03$, compared to a $\Delta h_f = 0.3$ for the $\Gamma = 0$ case.

Figure 11 illustrates the effect of various evaporation rates on the evolution of the coating layer during the drying−leveling process. Increasing the evaporation rate causes the difference in the resin concentrations between the crests and the troughs to increase at a faster rate, as shown by the (E/h) term in eq 22. Thus increasing the evaporation rate causes surface tension gradients to be developed earlier in the flow history, promoting leveling during the early times and deleveling after the coating height undergoes a reversal. But by increasing the resin concentration, we also increase the viscosity according to the exponential law in eq 23. By increasing the viscosity, we lower Q_{stg}, Q_{st}, and Q_g, slowing lateral movement of the liquid. These two counteracting mechanisms are illustrated in Figure 11. For the fast evaporation case, $E^{(0)} = 504$, strong surface tension gradients help to quickly level the initially uneven surface, but the corresponding increase in viscosity freezes the coating before it can completely level. For the $E^{(0)} = 168$, $E^{(0)} = 112$, and $E^{(0)} = 84$ cases the coating height undergoes one reversal, but the increase in viscosity with evaporation prohibits a second reversal (though surface tension gradients act to level the surface in the later time periods for all these cases). The coating height undergoes two reversals in the $E^{(0)} = 56$ case, yielding a positive Δh_f. For the $E^{(0)} = 28$ case, the coating height goes through three reversals, yielding a final negative Δh_f. For all $E^{(0)} \leq 28$ (not shown), the coating height undergoes three or more reversals, and $|\Delta h_f|$ is less than 0.02.

As in the Γ case considered above, these results indicate that there are several distinct ranges in $E^{(0)}$ for an optimal Δh_f, as shown in Figure 12. If we require $|\Delta h_f| \leq 0.05$, then $E^{(0)}$ must be within the ranges $422.0 \leq E^{(0)} \leq 495.0$ (in which case the surface will undergo at most one reversal) and $70.0 \leq E^{(0)} \leq 95.0$ (one or two reversals) and $0 < E^{(0)} \leq 45.0$ (two or more reversals). The maximum amplitude of $\Delta h(t)$ becomes smaller with every coating height reversal and, for sufficiently small $E^{(0)}$, we can ensure as small a Δh_f as desired. However, choosing a small evaporation rate is usually not desirable because it increases total production time.

The parameters Γ and $E^{(0)}$ control the final coating height variation of a drying−leveling coating. For a specific application, the evaporation rate $E^{(0)}$ is varied by increas-

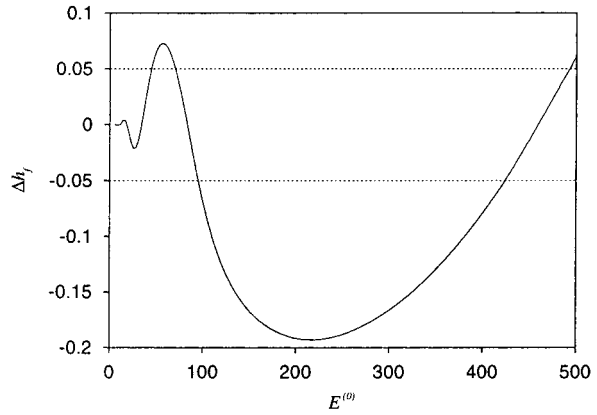

Figure 12. Difference in coating height between initial crests and initial troughs at the dry time Δh_f plotted versus $E^{(0)}$. Other dimensionless parameters are fixed and are given in Table 2. Also shown are the lines $\Delta h_f = -0.05$ and $\Delta h_f = 0.05$.

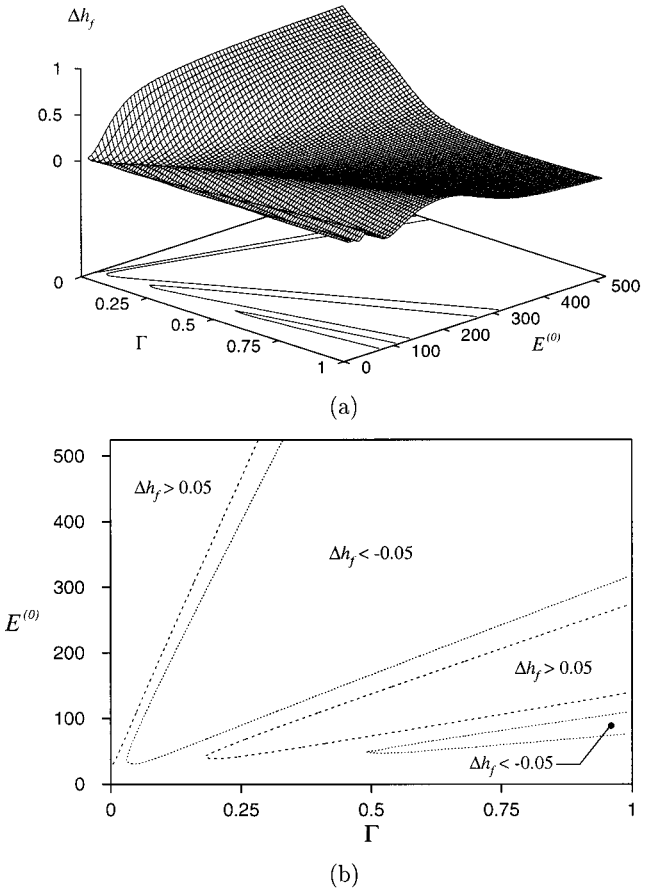

Figure 13. (a) Difference in coating height between initial crests and initial troughs at the dry time Δh_f plotted for a range of Γ and $E^{(0)}$ values. Other dimensionless parameters are fixed and are given in Table 2. (b) Contour lines are drawn for $|\Delta h_f| = 0.05$ to designate favorable operational ranges for Γ and $E^{(0)}$.

ing (or decreasing) the ambient temperature or by using a more (or less) volatile solvent. The parameter Γ is also varied by using different resins and/or solvents. In Figure 13 we show the final coating height difference Δh_f for different Γ and $E^{(0)}$ values. The regions which yield undesirable final coating height variations ($|\Delta h_f| > 0.05$) are marked in Figure 13b. The region where $E^{(0)}$ is less than 25 always yields an acceptable final coating height variation; nevertheless, such low evaporation rates are not desirable because of productivity constraints. For a given coating (Γ is fixed), it is possible to find a range of evaporation rates which yields $|\Delta h_f| < 0.05$ by using Figure 13b.

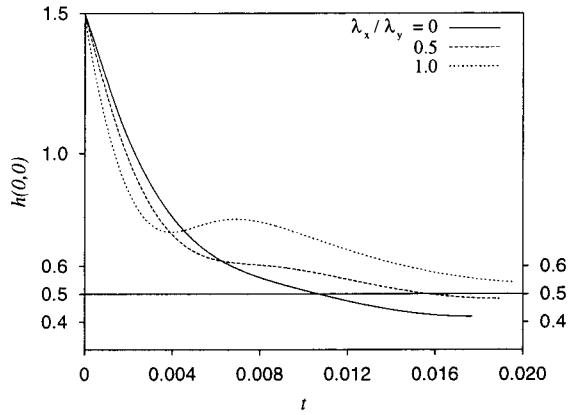

Figure 14. Coating height at the corner $h(0,0)$ as a function of time for various values of λ_x/λ_y. For the $\lambda_x/\lambda_y = 0$ case the profile is one-dimensional. For the $\lambda_x/\lambda_y = 0.5$ case the wavelength in the x direction is twice that in the y direction. The $\lambda_x/\lambda_y = 1$ case corresponds to our model simulation. Other dimensionless parameters are fixed and are given in Table 2. Each curve stops when all of the solvent has evaporated.

Figure 14 demonstrates the effect of different initial conditions on the history of the flow. The case $\lambda_x/\lambda_y = 0$ corresponds to a one-dimensional profile with $\tilde{\lambda}_{\tilde{x}} = 0.5$ cm. Because the surface is only curved in one dimension, the fluxes from Q_{st} are much lower for this case compared to the full three-dimensional coating height variation considered in the model simulation. The coating height undergoes one reversal at $t = 0.0023$, and the final $\Delta h(t)$ is negative: $\Delta h_f = -0.146$. For the $\lambda_x/\lambda_y = 0.5$ case, the increased surface curvature in the y direction encourages leveling. The coating height undergoes one reversal at $t = 0.0018$, and the final is again negative: $\Delta h_f = -0.037$. The $\lambda_x/\lambda_y = 1$ case corresponds to our model simulation. Here the increased leveling effects due to the larger Q_{st} cause a coating height reversal at $t = 0.0013$, and a second reversal at $t = 0.063$, and the final $\Delta h(t)$ is positive: $\Delta h_f = 0.073$.

6.4. Effect of Spatial Evaporation Gradients. In eq 24 the function f controls the evaporation rate by its explicit dependence on space and time. To illustrate the effect of uneven spatial evaporation rates, we choose f to be a two-dimensional Gaussian distribution function in the form of

$$f(x,y) = \exp[-(ax)^2 - (by)^2]$$

For $a = b$ the evaporation profile is axisymmetric. We start with a uniform initial coating height and resin concentration

$$h(x,y,t=0) = 1 \quad \text{and} \quad c(x,y,t=0) = 0.5.$$

Because the evaporation rate is higher at the corner region ($x = 0$, $y = 0$), the resin concentration increases faster there compared to the outer regions. This causes spatial gradients in resin concentration, yielding surface tension gradients which act to move liquid toward the corner region. In Figure 15 we plot final coating height profiles for three a/b ratios. For the axisymmetric case the flow induced by surface tension gradients in the x and y directions is the same; hence, the final coating profile is axisymmetric. As the ratio a/b decreases, the flow induced by surface tension gradients in the y direction dominates, leading to short-wavelength ripples in that direction.

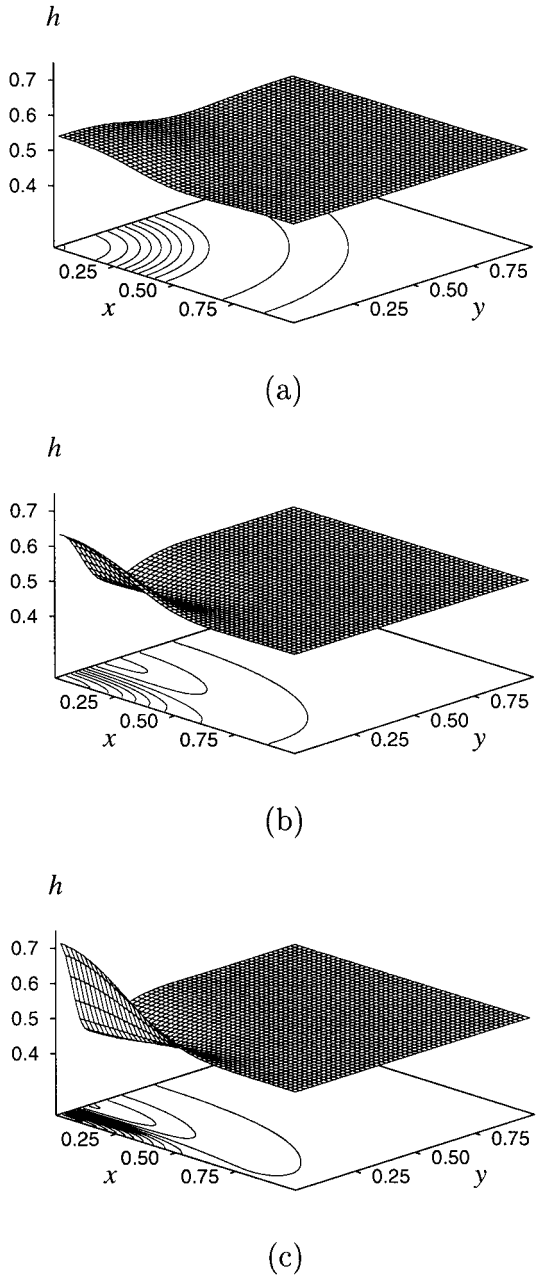

Figure 15. Effect of spatial evaporation gradients on an initially uniform coating layer. Final coating height profiles are shown for (a) $a/b = 1$, (b) $a/b = 0.4$, and (c) $a/b = 0.2$

6.5. Discussion. In this section we have used the linear solution to explain the interaction between spatial coating height and resin concentration gradients. We then examined results from a model simulation using parameters characteristic of an alkyd paint. We used several types of plots to explain the complex effects of surface tension gradient, surface tension, and gravitational forces during the drying−leveling process. The effects of changing two dimensionless parameters characterizing the coating liquid, Γ and $E^{(0)}$, show that there are distinct ranges for these parameters which lead to comparatively level final coating profiles. If the time scale for the viscosity increase due to solvent evaporation is adjusted with the time scale for surface-tension-gradient-induced oscillatory motion, it may be possible to "catch" the surface profile near a reversal time, resulting in a comparatively level final surface profile. Finally, the numerical study of the effect of λ_y showed the importance of three-dimensional effects on the leveling behavior of liquid coatings.

7. Conclusions

We have presented a mathematical model of a drying paint film on a two-dimensional, horizontal substrate. The paint is modeled as a multicomponent liquid with one volatile component and one nonvolatile component. The model includes such effects as lateral diffusion and convection of resin within the bulk liquid, temporal and spatial variations in the evaporation rate, viscosity and surface tension gradients due to compositional changes, and arbitrary initial coating thickness variations. By limiting consideration to thin liquid films with small free surface gradients and averaging all quantities across the thin layer, the governing equations are reduced to a pair of coupled, nonlinear, partial differential equations. These are solved using a partially implicit time-splitting method which requires a minimum of computational resources while retaining the essential nonlinear elements of the problem.

An approximate linearized solution to the governing partial differential equations is developed and is used to illustrate the relationship between spatial resin concentration and coating height variations. The numerical model and linearized solution agree well for slightly perturbed coating layers.

A sample simulation of the full nonlinear problem, using the coating properties of a typical alkyd paint, is used to illustrate the complex interactions of gravitational, surface tension, and surface-tension-gradient forces during the drying−leveling process. This simulation of the full nonlinear problem indicates that surface tension gradients arising from compositional changes can greatly affect the flow history of thin liquid coatings. For instance, when spatial evaporation gradients act on initially uniform coating layers, surface tension gradients due to compositional changes may cause irregularities in the final dry coating profile.

For films with irregularities in the initial coating height, solvent evaporation may lead to surface tension gradients which cause an oscillatory motion of the free surface. These surface tension gradients are not necessarily to be avoided. If the time scale for the viscosity increase of the bulk liquid due to solvent evaporation is matched with the time scale for surface-tension-gradient-induced oscillatory motion, surface tension gradients may be used to promote substantial leveling of an initially uneven coating layer. The results of our simulations suggest the existence of certain surface tension and evaporation rate values where the final coating thickness variation can be minimized.

Waterborne coatings have water as their main solvent and a low surface tension cosolvent. In cases where the cosolvent evaporates faster than the water, the "rebound" effect was observed in recent studies.[3,4] Our mathematical and numerical model can also be applied to the analysis of the leveling of waterborne coatings.

Acknowledgment. This work is supported by the ICI Strategic Research Fund, the NASA Microgravity Program, and the State of Delaware Research Partnership Program.

LA980414U